XIV International Conference on Computational Plasticity. Fundamentals and Applications
COMPLAS XIV
E. Oñate, D.R.J. Owen, D. Peric & M. Chiumenti (Eds)

EXPLICIT FINITE ELEMENT IMPLEMENTATION OF A SHAPE MEMORY ALLOY CONSTITUTIVE MODEL AND ASSOCIATED ANALYSES

G. Scalet[°,*], E. Boatti[†], M. Ferraro[§], V. Mercuri[°], D.J. Hartl[^] and F. Auricchio[°]

[°] Dipartimento di Ingegneria Civile e Architettura
Università di Pavia
Via Ferrata 3, 27100 Pavia, Italy
e-mail: giulia.scalet@unipv.it/ valentina.mercuri01@universitadipavia.it / auricchio@unipv.it

[†]John A. Paulson School of Engineering and Applied Sciences
Harvard University
Cambridge, MA 02138, USA
e-mail: eboatti@seas.harvard.edu

[§]Institute of Bioengineering
École Polytechnique Fédérale de Lausanne, EPFL
BM 5125 Lausanne 1015, Switzerland
e-mail: mauro.ferraro@epfl.ch

[^]Department of Aerospace Engineering
Texas A&M University
College Station, TX 77843-3409, USA
e-mail: darren.hartl@tamu.edu

Key words: Shape memory alloys, Pseudoelasticity, Shape memory effect, Explicit integration, Constitutive modeling

Abstract. Shape memory alloys (SMA) represent an important class of smart metallic materials employed in various innovative applications thanks to their unique thermomechanical behavior. Since the 1980s, several SMA constitutive models have been proposed and implemented into both commercial and academic finite element analysis software tools. Such models have demonstrated their reliability and robustness in the design and optimization of a wide variety of SMA-based components. However, most models are implemented using implicit integration schemes, thus limiting their applicability in highly nonlinear analyses. The objective of this work is to present a novel explicit integration scheme for the numerical implementation of the three-dimensional Souza-Auricchio model, a phenomenological model able to reproduce the primary SMA responses (i.e., pseudoelasticity and shape memory effect). The model constitutive equations are formulated by adopting the continuum thermodynamic theory with internal variables, following a plasticity-like approach. An elastic predictor-inelastic corrector scheme is here used to

solve the time-discrete non-linear constitutive equations in the explicit framework. The proposed algorithm is investigated through several benchmark boundary-value problems of increasing complexity, considering both pseudoelastic and shape memory response in quasi-static conditions; a comparison with an implicit integration scheme is also performed. Such numerical tests demonstrate the ability of the algorithm to reproduce key material behaviors with effectiveness and robustness. Particularly, the analysis of SMA cables demonstrates the effectiveness of the explicit algorithm to solve complex problems involving widespread nonlinear contact, which prevent the convergence of the implicit scheme. Details such as mass-scaling options are also discussed.

1 INTRODUCTION

In the last three decades the utilization of shape memory alloys (SMA) has evolved from academic and niche applications to the mass production of a wide variety of industrial components. The great commercial success of SMA is due to two unique mechanical properties: pseudoelasticity and shape memory effect. These features have enabled a wide range of commercial applications, e.g., biomedical devices, civil engineering components, and mechanical systems [1]. Several efforts have been made during the past years to propose reliable constitutive models for SMA to be incorporated in numerical analysis tools, which can be generally categorized as microscopic, macroscopic, or micro-macro (see, e.g., [2, 3] for a review). This paper focuses on macroscopic ones, widely employed because of their simple numerical implementation and reduced cost of calculation.

Most of the phenomenological models available in the literature are implemented in an implicit time integration framework, with only few recent contributions utilizing an explicit alternative [4, 5, 6]. As well known, the employment of explicit methods becomes truly enabling in cases where complexity makes implicit algorithms impractical, such as in high-speed/non-linear dynamic analyses or in fully coupled thermo-mechanical dynamic analyses, which characterize several SMA applications.

The present paper aims to improve the current state-of-the-art regarding explicit implementation of SMA models within the general-purpose commercial Finite Element Analysis (FEA) solver Abaqus by proposing an explicit integration scheme for the three-dimensional phenomenological model presented in [7, 8], and defined in the following as the *Souza-Auricchio model*. This model has been chosen because of its extremely simple solution scheme and its ability in describing both of pseudoelastic and shape memory behaviors. In fact, it represents an improvement over the Auricchio-Taylor-Lubliner [9] model, which is currently available as built-in subroutine in Abaqus but it is not able to reproduce the zero-stress shape memory effect.

The present study provides a detailed description of the explicit integration scheme for the Souza-Auricchio model and an in-depth investigation of the corresponding algorithm. The constitutive and algorithmic framework is tested via the simulation of two complex three-dimensional boundary-value problems and compared to the implicit scheme as proposed in [8]. The first one assesses thermally-induced actuation problems through the

study of a SMA micro-gripper for micro-parts manipulation; while the pseudoelastic effect is investigated through a SMA cable segment, where widespread frictional contact among twisted SMA wires can be exploited for applications in civil and seismic engineering.

2 Souza-Auricchio model: time-continuous formulation

The present section briefly reviews the time-continuous formulation of the Souza-Auricchio model. The reader is referred to [7, 8] for further details.

The control variables are the total strain $\boldsymbol{\varepsilon}$ and the absolute temperature T, while the internal variable is transformation strain $\boldsymbol{e^{tr}}$. The Helmoltz free energy function is expressed as follows:

$$\Psi = \frac{1}{2}\,\kappa\,\theta^2 + G\,\|\boldsymbol{e} - \boldsymbol{e^{tr}}\|^2 + \tau_M\,\|\boldsymbol{e^{tr}}\| + \frac{1}{2}\,h\,\|\boldsymbol{e^{tr}}\|^2 + \mathcal{I}_{\varepsilon_L}(\boldsymbol{e^{tr}})\ . \tag{1}$$

Here, θ and $\boldsymbol{e}$ are the volumetric and deviatoric part of $\boldsymbol{\varepsilon}$, respectively; $\tau_M = \beta\langle T - T^*\rangle$, where β is a positive parameter and T^* is a reference temperature; κ and G are the bulk and shear modulus, respectively; h defines the phase transformation hardening. The indicator function

$$\mathcal{I}_{\varepsilon_L}(\boldsymbol{e}^{tr}) = \begin{cases} 0 & \text{if } \|\boldsymbol{e}^{tr}\| \le \varepsilon_L \\ +\infty & \text{otherwise} \end{cases} \tag{2}$$

is introduced to satisfy the transformation strain constraint $\|\boldsymbol{e}^{tr}\| \le \varepsilon_L$.

The constitutive equations are found to be:

$$\begin{aligned} \boldsymbol{s} &= \frac{\partial \Psi}{\partial \boldsymbol{e}} = 2G(\boldsymbol{e} - \boldsymbol{e}^{tr})\ , \\ \boldsymbol{X} &= -\frac{\partial \Psi}{\partial \boldsymbol{e}^{tr}} = \boldsymbol{s} - \tau_M \frac{\boldsymbol{e}^{tr}}{\|\boldsymbol{e}^{tr}\|} - h\boldsymbol{e}^{tr} - \gamma \frac{\boldsymbol{e}^{tr}}{\|\boldsymbol{e}^{tr}\|}\ , \end{aligned} \tag{3}$$

where $\boldsymbol{s}$ is the deviatoric part of $\boldsymbol{\sigma}$ and $\boldsymbol{X}$ is the thermodynamic force associated to $\boldsymbol{e}^{tr}$. The variable γ results from the subdifferential $\partial\mathcal{I}_{\varepsilon_L}(\boldsymbol{e}^{tr})$ and it is defined as follows:

$$\gamma = \begin{cases} 0 & \text{if } \|\boldsymbol{e}^{tr}\| < \varepsilon_L \\ \ge 0 & \text{if } \|\boldsymbol{e}^{tr}\| = \varepsilon_L \end{cases}\ , \tag{4}$$

with $\partial\mathcal{I}_{\varepsilon_L}(\boldsymbol{e}^{tr}) = \gamma \boldsymbol{e}^{tr}/\|\boldsymbol{e}^{tr}\|$.

To describe phase transformation and inelasticity evolution, a classical Mises-type limit function is introduced in the following form:

$$F = \|\boldsymbol{X}\| - R_Y\ , \tag{5}$$

where R_Y is a positive material parameter.

The evolution equation for the internal variable takes the form:

$$\dot{\boldsymbol{e}}^{tr} = \dot{\lambda}\frac{\partial F}{\partial \boldsymbol{X}} = \dot{\lambda}\frac{\boldsymbol{X}}{\|\boldsymbol{X}\|}\ , \tag{6}$$

where $\dot{\lambda}$ is the non-negative consistency parameter. The model is then completed by the classical Kuhn-Tucker conditions:

$$\dot{\lambda} \geq 0, \quad F \leq 0, \quad \dot{\lambda} F = 0 \, . \tag{7}$$

3 Souza-Auricchio model: time-discrete formulation

We now focus on the algorithmic treatment of the continuum model equations in an explicit framework. In the following we use subscript n for the variables at previous time t_n and we drop subscript *n+1* for the variables at current time t_{n+1}. We make use of a forward Euler scheme foor the evolution equation (6), as follow:

$$\boldsymbol{e}^{tr} = \boldsymbol{e}^{tr}_n + \Delta\lambda \frac{\boldsymbol{X}_n}{\|\boldsymbol{X}_n\|} \, , \tag{8}$$

where $\Delta\lambda = \int_{t_n}^{t_{n+1}} \dot{\lambda} \;\; dt$. The proposed algorithm is provided in Table 1. An elastic predictor/inelastic corrector scheme is adopted to compute the variables at the current time t_{n+1} based on the quantities at the previous time t_n: if the trial state is admissible, the step is elastic; otherwise, the step is inelastic and the transformation strain must be updated through the time-discrete evolution equation (8). We compute the inelastic increment (referred to as the *first phase transformation* or *PT1 step* in Table 1) to evaluate the consistency parameter $\Delta\lambda$. We derive the needed relation for $\Delta\lambda$ by enforcing the consistency condition $F(\Delta\lambda) = 0$. The consistency parameter $\Delta\lambda = \Delta\lambda_{PT1}$ is explicitly derived by applying a single iteration of the Newton-Raphson scheme to the consistency condition, as follows:

$$\Delta\lambda_{PT1} = \Delta\lambda^{(0)} + \delta\Delta\lambda^{(0)} = \Delta\lambda^{(0)} - \left(\left. \frac{dF}{d\Delta\lambda} \right|^{(0)} \right)^{-1} F^{(0)} \, , \tag{9}$$

where we consider:

$$\begin{cases} \Delta\lambda^{(0)} = \Delta\lambda_{TR} = 0 \\ F^{(0)} = F_{TR} \\ \left. \dfrac{dF}{d\Delta\lambda} \right|^{(0)} = \left. \dfrac{dF}{d\Delta\lambda} \right|_{TR} \end{cases} \, . \tag{10}$$

The derivative $dF/d\Delta\lambda$ is therefore computed as:

$$\left. \frac{dF}{d\Delta\lambda} \right|_{TR} = \frac{\boldsymbol{X}_{TR}}{\|\boldsymbol{X}_{TR}\|} : \left\{ -(2G+h)\mathbb{I} - \frac{\tau_M}{\|\boldsymbol{e}^{tr}_{TR}\|} \left[\mathbb{I} - \frac{\boldsymbol{e}^{tr}_{TR} \otimes \boldsymbol{e}^{tr}_{TR}}{\|\boldsymbol{e}^{tr}_{TR}\|} \right] \right\} : \frac{\boldsymbol{X}_{TR}}{\|\boldsymbol{X}_{TR}\|} \, , \tag{11}$$

where $\mathbb{I}$ is the fourth order identity tensor. Then, we can derive the transformation strain, as follows:

$$\boldsymbol{e}^{tr}_{PT1} = \boldsymbol{e}^{tr}_n + \Delta\lambda_{PT1} \frac{\boldsymbol{X}_{TR}}{\|\boldsymbol{X}_{TR}\|} \, . \tag{12}$$

After the inelastic step is performed, a check is made on the transformation strain constraint. If the constraint is not satisfied, a further inelastic step (referred to as the *second phase transformation* or *PT2 step* in Table 1) is performed, where the transformation strain $\boldsymbol{e}^{tr} = \boldsymbol{e}^{tr}_{PT2}$ is calculated starting from the PT1 step solution, as follow:

$$\boldsymbol{e}^{tr}_{PT2} = \varepsilon_L \frac{\boldsymbol{e}^{tr}_{PT1}}{\|\boldsymbol{e}^{tr}_{PT1}\|} \, . \tag{13}$$

Such an approximation allows for a simplified calculation and reduced number of functional evaluations for each time increment, but small increments are required. From Eqs (5) and (6) we obtain:

$$\boldsymbol{X} = R_Y \frac{\boldsymbol{e}^{tr} - \boldsymbol{e}^{tr}_n}{\overline{\|\boldsymbol{e}^{tr} - \boldsymbol{e}^{tr}_n\|}} \, . \tag{14}$$

Combining Eqs (13), (14) and $(3)_2$, we obtain the following relation:

$$R_Y \frac{\boldsymbol{e}^{tr}_{PT2} - \boldsymbol{e}^{tr}_n}{\overline{\|\boldsymbol{e}^{tr}_{PT2} - \boldsymbol{e}^{tr}_n\|}} - 2G\left(\boldsymbol{e} - \boldsymbol{e}^{tr}_{PT2}\right) + \tau_M \frac{\boldsymbol{e}^{tr}_{PT2}}{\|\boldsymbol{e}^{tr}_{PT2}\|} + h\boldsymbol{e}^{tr}_{PT2} + \gamma_{PT2} \frac{\boldsymbol{e}^{tr}_{PT2}}{\|\boldsymbol{e}^{tr}_{PT2}\|} = 0 \, , \tag{15}$$

from which we derive the saturation coefficient $\gamma = \gamma_{PT2}$:

$$\gamma_{PT2} = \left(-R_Y \frac{\boldsymbol{e}^{tr}_{PT2} - \boldsymbol{e}^{tr}_n}{\overline{\|\boldsymbol{e}^{tr}_{PT2} - \boldsymbol{e}^{tr}_n\|}} + 2G\left(\boldsymbol{e} - \boldsymbol{e}^{tr}_{PT2}\right) - \tau_M - h\boldsymbol{e}^{tr}_{PT2} \right) : \frac{\boldsymbol{e}^{tr}_{PT2}}{\|\boldsymbol{e}^{tr}_{PT2}\|} \, . \tag{16}$$

where $\overline{\|\boldsymbol{e}^{tr} - \boldsymbol{e}^{tr}_n\|}$ is the regularized expression. The proposed algorithm is simple to implement. Compared to [6], our procedure does not include a convergence criterion to determine $\Delta\lambda_{PT1}$, thus making it truly explicit, compatible with the global explicit scheme, and allowing a low computational cost per increment. Similarly, the computation of γ_{PT2} is straightforward, contrary to the method of [6], which proposed a linearization and then an iterative procedure for the PT2 step. Finally, unlike the implicit scheme, the explicit algorithm does not require the often expensive computation of a tangent matrix, consistent or otherwise.

4 Numerical simulations

We now test the performance of the proposed algorithm, which is implemented within Abaqus/Explicit through a VUMAT user subroutine. A comparison with the implicit scheme, implemented within Abaqus/Standard through a UMAT user subroutine, is provided [8]. In particular, we use the package AceGen of the symbolic software Mathematica to generate the numerical subroutines for Abaqus. All bodies considered are discretized into first-order hexahedral elements with full and reduced integration, respectively, for the implicit and explicit method. Since the explicit method is here used to solve quasi-static problems, we employ the method of mass scaling to reduce the simulation runtime. To avoid inflation of the mass and oscillations during the quasi-static solution, we carefully check that the kinetic energy was below 5-10% of the internal energy. In all numerical studies we adopt the material parameters reported in Table 2.

Table 1: Explicit algorithm proposed for the Souza-Auricchio model.

Given quantities: $\boldsymbol{\varepsilon}, T, \boldsymbol{e}_n^{tr}, \Delta\lambda_n, \gamma_n$

Compute trial state:

$\Delta\lambda_{TR} = 0$; $\boldsymbol{e}_{TR}^{tr} = \boldsymbol{e}_n^{tr}$; $\gamma_{TR} = 0$

$\boldsymbol{s}_{TR} = 2G\left(\boldsymbol{e} - \boldsymbol{e}_{TR}^{tr}\right)$

$\boldsymbol{X}_{TR} = \boldsymbol{s}_{TR} - \tau_M \dfrac{\boldsymbol{e}_{TR}^{tr}}{\|\boldsymbol{e}_{TR}^{tr}\|} - h\boldsymbol{e}_{TR}^{tr}$

$F_{TR} = \|\boldsymbol{X}_{TR}\| - R_Y$

IF $F_{TR} \leq tol$ THEN

Elastic step:

$\Delta\lambda = \Delta\lambda_{TR}$; $\boldsymbol{e}^{tr} = \boldsymbol{e}_{TR}^{tr}$; $\gamma = \gamma_{TR}$; $\boldsymbol{s} = \boldsymbol{s}_{TR}$; $\boldsymbol{X} = \boldsymbol{X}_{TR}$

ELSE

Inelastic step:

Compute $\Delta\lambda_{PT1}$ via Eq. (9)

$\boldsymbol{e}_{PT1}^{tr} = \boldsymbol{e}_n^{tr} + \Delta\lambda_{PT1} \dfrac{\boldsymbol{X}_{TR}}{\|\boldsymbol{X}_{TR}\|}$

IF $\|\boldsymbol{e}_{PT1}^{tr}\| \leq \varepsilon_L$ THEN

$\Delta\lambda = \Delta\lambda_{PT1}$; $\boldsymbol{e}^{tr} = \boldsymbol{e}_{PT1}^{tr}$; $\gamma = \gamma_{TR}$

$\boldsymbol{s} = 2G\left(\boldsymbol{e} - \boldsymbol{e}^{tr}\right)$

$\boldsymbol{X} = \boldsymbol{s} - \tau_M \dfrac{\boldsymbol{e}^{tr}}{\|\boldsymbol{e}^{tr}\|} - h\boldsymbol{e}^{tr}$

ELSE

Saturation step:

$\boldsymbol{e}^{tr} = \boldsymbol{e}_{PT2}^{tr} = \varepsilon_L \dfrac{\boldsymbol{e}_{PT1}^{tr}}{\|\boldsymbol{e}_{PT1}^{tr}\|}$

Compute $\gamma = \gamma_{PT2}$ via Eq. (16)

$\boldsymbol{s} = 2G\left(\boldsymbol{e} - \boldsymbol{e}^{tr}\right)$

$\boldsymbol{X} = \boldsymbol{s} - \left(\tau_M + \gamma\right) \dfrac{\boldsymbol{e}^{tr}}{\|\boldsymbol{e}^{tr}\|} - h\boldsymbol{e}^{tr}$

END IF

END IF

Table 2: Adopted material parameters for the Souza-Auricchio model (taken from [10]).

Description	Symbol	Value	Unit
Young's modulus	E	53,000	MPa
Poisson's ratio	ν	0.33	-
Stress-strain slope during transformation	h	1,000	MPa
Maximum axial transformation strain	ε_L	0.056	-
Reference temperature	T^*	243	K
Term related to $\tau_M = \beta(T - T^*)^+$	β	6.1	MPa/K
Elastic domain radius in the deviatoric stress space	R_Y	100	MPa

4.1 Actuation of a micro-gripper

The adopted geometry for the SMA micro-gripper is shown in Figure 1 which reports the adopted reference mesh, consisting of 14, 376 elements and 24, 417 nodes.

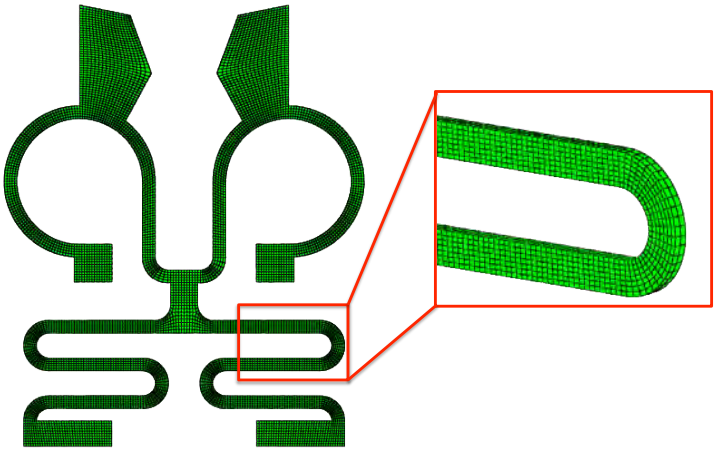

Figure 1: SMA micro-gripper: mesh and initial geometry.

The micro-gripper operates via a complex antagonistic actuation cycle, as shown in Figure 2. The gripper is divided in two actuation units: the upper part, actually devoted to the action of gripping, is referred to as the *rotational stage*; the lower part, which stretches and contracts, is referred to as the *linear stage*. The four small quadrilateral features in Figure 2 are referred to as *tabs*. During the full working cycle, the tabs of the *linear stage* are fully constrained (steps A-C of Figure 2). At the beginning of the actuation cycle, the gripper is at low temperature. In step A, a displacement v of 2.5 mm is applied to the region connecting the two stages, and the linear stage is stretched. During step B, the tabs of the *rotational stage* are fully constrained and the linear stage is heated; it thus tends to recover its original configuration and contracts (the direction is indicated by the black arrow in step B). The contraction of the linear stage combined with the full constraint on the four tabs produces the gripping action (clockwise rotation of the rotational part in step B). Finally, during step C, the linear stage is cooled down, and

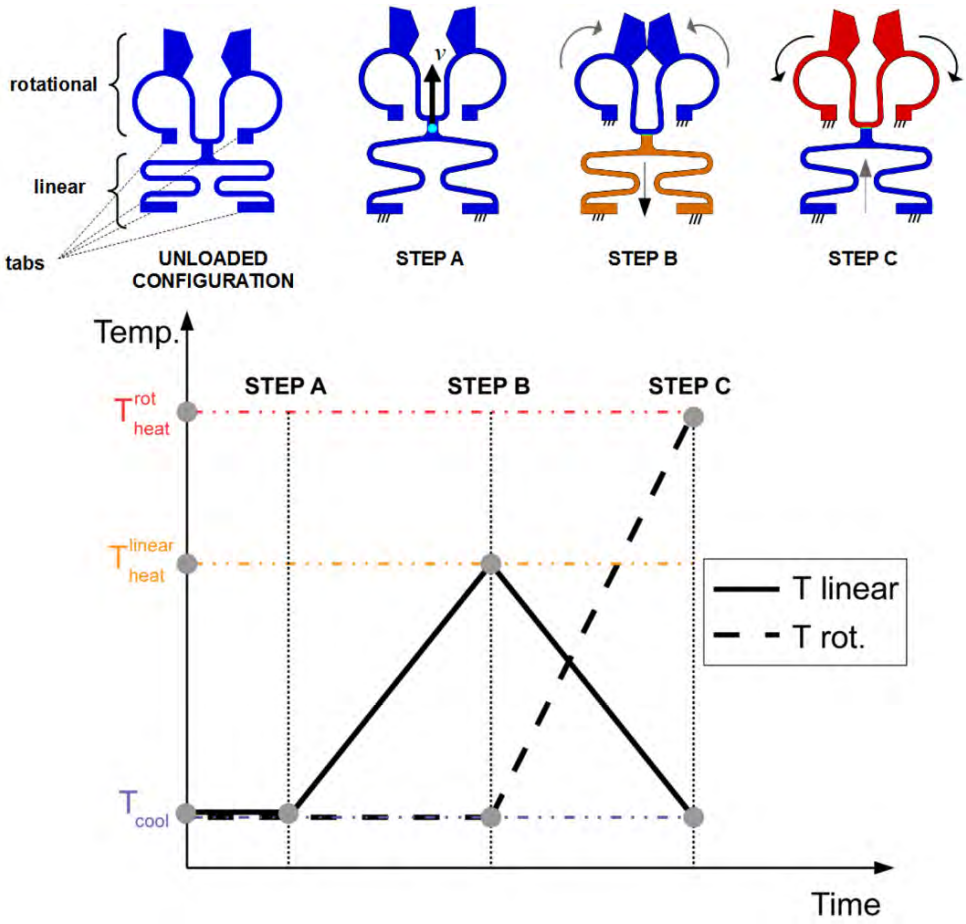

Figure 2: SMA micro-gripper: (above) working principle; (below) trends of the temperature T over time. T *linear* is the temperature history for the linear stage, while T *rot* is the temperature history for the rotational stage.

the rotational stage is heated; it thus recovers its initial shape, reaching the open position (anti-clockwise rotation in step C). As the rotational stage moves, it forces the linear stage to stretch (the direction is indicated by the grey arrow in step C). Figure 3 shows the deformed state of the micro-gripper and contour plots of the transformation strain norm at steps B and C for both implicit and explicit analyses. Since a different element integration type has been used in the implicit and explicit analyses, it can be noted that some difference exists between the two deformed shapes at state B; moreover, some very small concentrations of transformation strain are observable in the highly curved regions of the micro-gripper in the case of the implicit analysis results.

In the explicit analysis, the stable time increment evaluated by Abaqus at the beginning of the analysis is $9.64 \cdot 10^{-9}$ s. Mass scaling is here applied in such a way that the minimum stable time increment (and the used time increment) can be set to 10^{-8} s. During the implicit analysis, the time increment is set to 10^{-2} s.

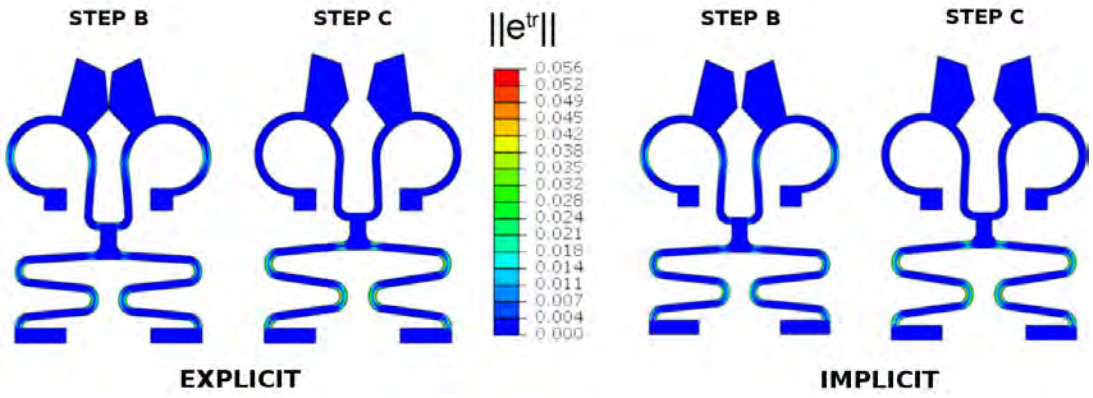

Figure 3: SMA micro-gripper: deformed shape of the gripper for implicit and explicit analyses at steps B and C of Figure 2. The contour plot of the transformation strain norm is displayed.

4.2 Pseudoelastic SMA cable

We analyze a structural cable model consisting of SMA wire assemblies as used in the development of a vibration absorber. The model considers a three layer straight cable segment having a total diameter of 30 mm. The relatively simple cable is composed by a central straight wire (core) and two layers helically wrapped around the core. The adopted discretization is reported in Figure 4 and consists of $323,158$ solid brick elements and $416,357$ nodes.

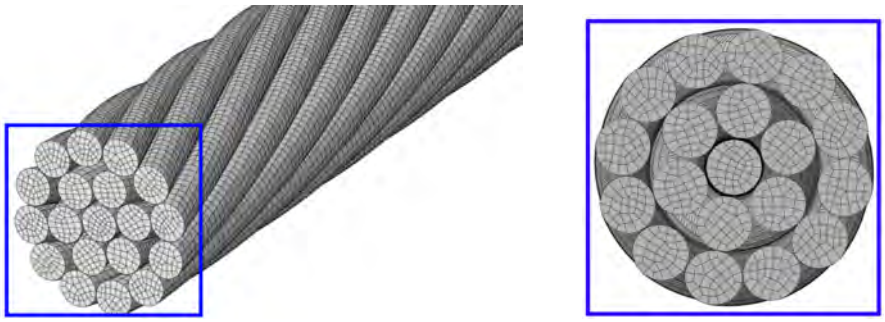

Figure 4: SMA cable: adopted mesh.

Following [11], our goal is to describe a hysteretic load-displacement cycle in the transverse direction Y preceded by a pretension phase along the longitudinal direction Z (Figure 5a-b). Contacts between the many wires exist and must be taken into account. To do so, a penalty formulation with Coulomb model is employed using a friction coefficient equal to 0.5. In this complex contact, the implicit iterative solver encounters a highly non-linear response and it attempts increasingly small time increments to solve the equilibrium equations, without achieving equilibrium and convergence. Therefore, a natural alternative to solve such problems is via an explicit approach. The stable time increment, evaluated by Abaqus at the beginning of the analysis, is $1.12 \cdot 10^{-8}$ s. Mass scaling is applied considering a fixed time increment of 10^{-7} s. The kinetic energy, despite some

oscillations, remains negligible, validating the appropriateness of the mass scaling for a hypothesis of quasi-static conditions. Figure 5c presents the hysteretic load displacement

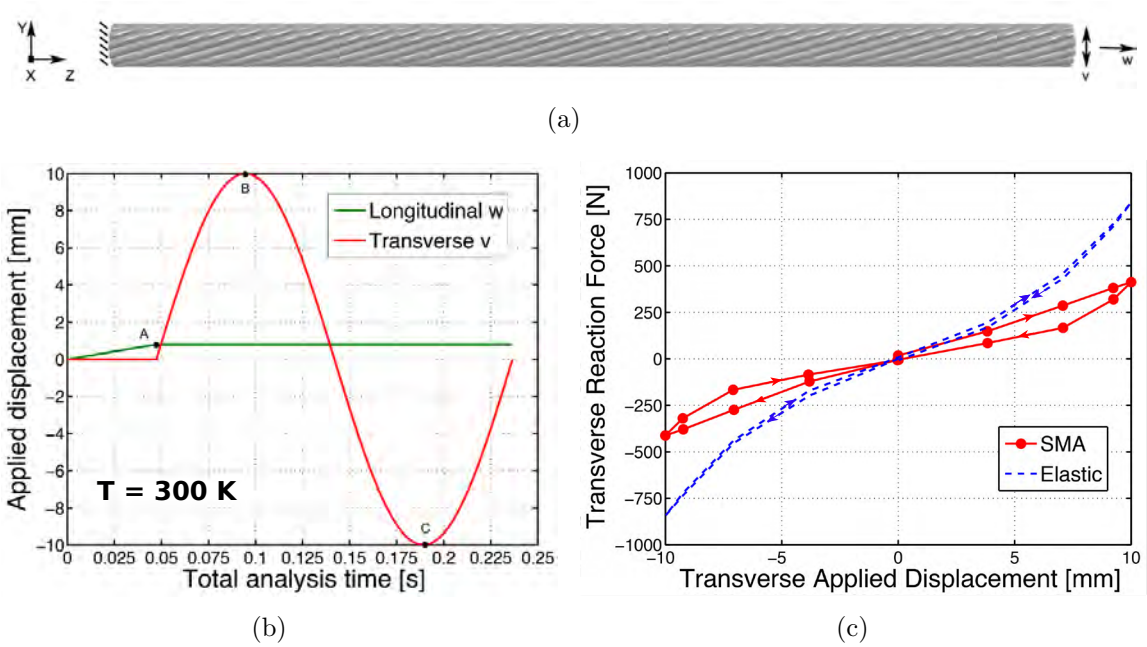

Figure 5: SMA cable: (a) applied boundary conditions; (b) loading history in terms of displacements. A total of 0.2364336 time units are used; (c) transverse force-displacement diagram.

relationship evaluated at the free end of the cable. A comparison with the curve obtained for an elastic cable with the same elastic properties is also provided. The responses are clearly different and evidence the hysteretic area obtained by using the SMA cable, which correspond to a gain in term of dissipatiton. Figure 6 shows the contour plot of the Von Mises stress evaluated at the mid section of the cable during pretension (a), maximum displacement (b), and minimum displacement (c) loading stages. Figure 7 shows the contour plot of the norm of the transformation strain at instant B of Figure 5. The figure clearly highlights that phase transformation is taking place: the transformation is complete close to the section where the load is applied and it is partial in most part of the core of the cable.

5 CONCLUSIONS

The present paper has proposed a novel implementation of the three-dimensional phenomenological Souza-Auricchio model using an explicit framework. A comparison of output results with the implicit integration scheme has also been made whenever possible. The explicit implementation has successfully simulated the quasi-static response of the considered devices. Particularly, the analysis of SMA cable has demonstrated the effectiveness of the explicit algorithm to solve complex problems involving widespread nonlinear contact. The results show the potential of the proposed computational framework to provide a virtual engineering tool for design, simulation, and optimization of SMA devices.

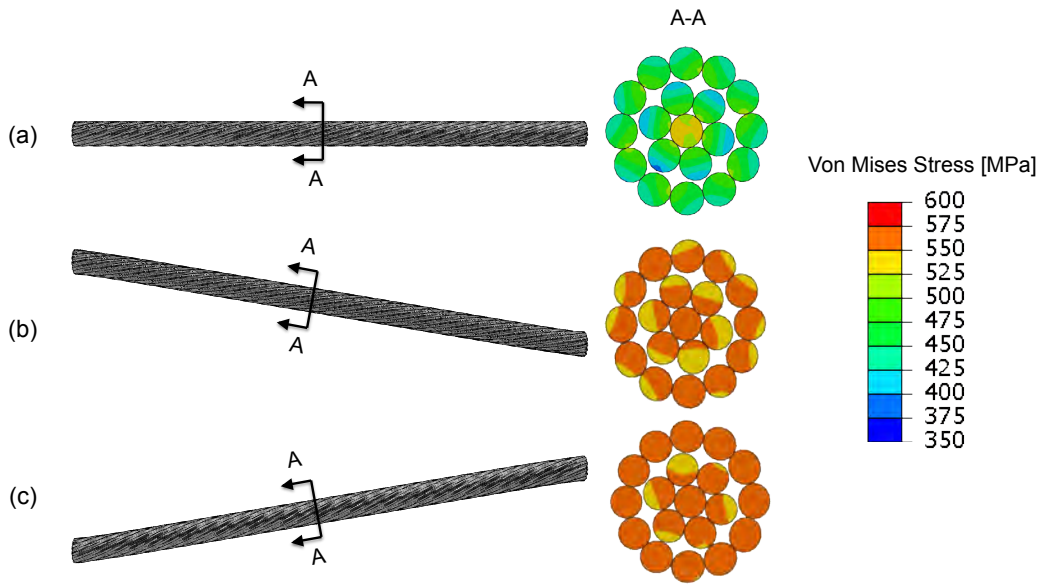

Figure 6: SMA cable: contour plot of the Von Mises stress at istants A, B, and C of Figure 5.

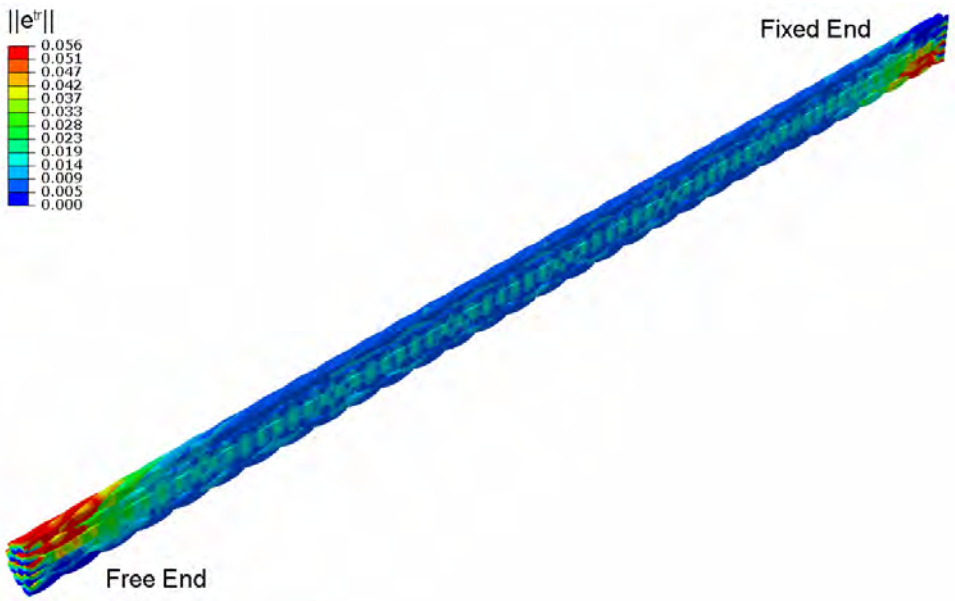

Figure 7: SMA cable: contour plot of the transformation strain norm at instant B of Figure 5.

Additionally, since SMA modeling techniques are continuously evolving, understanding the nature, advantages, and disadvantages of both implicit and explicit methods is helpful in choosing the right algorithm for the problem under investigation. Future developments will use the proposed explicit algorithm for high-speed dynamic simulations which are

widely exploited in SMA-based seismic or impact applications.

REFERENCES

[1] Jani, J., Leary, M., Subic, A. and Gibson, M. A review of shape memory alloy research, applications and opportunities. *Mater Design.* (2014) **56**: 1078-1131.

[2] Cisse, C., Zaki, W. and Zineb, T.B. A review of constitutive models and modeling techniques for shape memory alloys. *Int. J. Plasticity.* (2016) **76**: 244-284.

[3] Khandelwal, A. and Buravalla., V. Models for shape memory alloy behavior: An overview of modeling approaches. *Int. J. Struct. Changes Solids.* (2009) **1**: 111-148.

[4] Scalet, G., Auricchio, F. and Hartl, D. Efficiency and effectiveness of implicit and explicit approaches for the analysis of shape-memory alloy bodies. *J. Intel. Mat. Syst. Str* (2015) **27**: 384-402.

[5] Stebner, A. and Brinson, L. Explicit finite element implementation of an improved three dimensional constitutive model for shape memory alloys. *Comput. Method. App. M.* (2013) **257**: 17-35.

[6] Jähne, R., *Multiaxial mechanical characterization and constitutive modeling of superelastic sheets for solid-state hinges.* Ph.D. thesis, ETH Zurich (2012).

[7] Souza, A., Mamiya, E. and Zouain, N. Three-dimensional model for solids undergoing stress-induced phase transformations. *Eur. J. Mech. A/Solids.* (1998) **17**: 789-806.

[8] Auricchio, F. and Petrini, L. A three-dimensional model describing stress-temperature induced solid phase transformations: solution algorithm and boundary value problems. *Int. J. Numer. Meth. Eng.* (2004) **61**: 807-836.

[9] Auricchio, F. and R. L. Taylor R. L. Shape-memory alloys: Modelling and numerical simulation of the finite-strain superelastic behavior. *Comput. Method. App. M.* (1997) **143**: 175-194.

[10] Auricchio, F., Morganti, S. and Reali, A. SMA numerical modeling versus experimental results. *Proc. Europ. Symp. on Martensitic Transformations* ESOMAT (2009): 1-6.

[11] Carboni, B., Lacarbonara, W. and Auricchio, F. Hysteresis of multiconfiguration assemblies of nitinol and steel strands: Experiments and phenomenological identification. *J. Eng. Mech.* (2014) **141**: 04014135.